Nuclear Instruments and Methods in Physics Research A 780 (2015) 27–32

Contents lists available at ScienceDirect

Nuclear Instruments and Methods in Physics Research A

journal homepage: www.elsevier.com/locate/nima

Model for neutron total cross-section at low energies for nuclear grade graphite

V.M. Galván Josa [a], J. Dawidowski [b,*], J.R. Santisteban [b], F. Malamud [b], R.G. Oliveira [c]

[a] Consejo Nacional de Investigaciones Científicas y Técnicas (CONICET), FaMAF, Universidad Nacional de Córdoba, Argentina
[b] Consejo Nacional de Investigaciones Científicas y Técnicas (CONICET), Comisión Nacional de Enegía Atómica-Universidad Nacional de Cuyo, Argentina
[c] Consejo Nacional de Investigaciones Científicas y Técnicas (CONICET), CIQUIBIC, Fac. Cs. Químicas, Universidad Nacional de Córdoba, Argentina

ARTICLE INFO

Article history:
Received 19 September 2014
Received in revised form
28 November 2014
Accepted 15 January 2015
Available online 23 January 2015

Keywords:
Small Angle Neutron Scattering
Small Angle X-ray Scattering
Porosity
Graphite

ABSTRACT

At subthermal neutron energies, polycrystalline graphite shows a large total cross-section due to small angle scattering processes. In this work, a new methodology to determine pore size distributions through the neutron transmission technique at subthermal energies is proposed and its sensitivity is compared with standard techniques. A simple model based on the form factor for spherical particles, normally used in the Small Angle Neutron Scattering technique, is employed to calculate the contribution of small angle effect to the total scattering cross-section, with the width and center of the radii distributions as free parameters in the model. Small Angle X-ray Scattering experiments were performed to compare results as a means to validate the method. The good agreement reached reveals that the neutron transmission technique is a useful tool to explore small angle scattering effects. This fact can be exploited in situations where large samples must be scanned and it is difficult to investigate them with conventional methods. It also opens the possibility to apply this method in energy-resolved neutron imaging. Also, since subthermal neutron transmission experiments are perfectly feasible in small neutron sources, the present findings open new possibilities to the work done in such kind of facilities.

1. Introduction

Advanced materials have nowadays a wide variety of applications in rapid development, like in the storage of information in magnetic disks, or in improvements in the mechanical properties of steel, high-impact plastics and super alloys and the current carrying in superconductors. The properties of these materials are critically determined by their structure at nanometric scale. Supported by this technological interest, a method to explore the bulk structure in a fast way which gained relevance in recent times is the thermal neutron transmission technique [1]. With the same rationale, the subthermal neutron transmission has been employed to study nanometric structures, as recently tested for the first time in graphite [2] (a material of great interest in nuclear industry), as an alternative to the well-known Small Angle Neutron Scattering technique. The total cross-section of subthermal neutrons in graphite had been repeatedly measured by different research teams in the last few decades, revealing that for neutrons of energies below 0.0018 eV (i.e. slightly less than that of the first Bragg edge) the experimental value varies from 4 to 8 barns, depending on the porosity level. In contrast, calculations using standard theoretical models that compute the crystal structure, but not the structure at nanometric scale (as employed in the nuclear data processing code NJOY [3]), produce a value of 0.2 barns. Recent experimental studies [2] have shown that this difference in the total cross-section is due to neutrons scattered at small angles, i.e. refractions and reflections in the great number of existent solid/air interfaces due to the graphite porosity, not taken into account by NJOY.

Graphite is widely used in nuclear installations, due to its ability to moderate fast neutrons and reflect slow neutrons. Examples are the proposed nuclear fuel made of graphite balls containing uranium oxycarbide or uranium dioxide employed in Very High-Temperature Gas reactors (one of the reactor concepts for the next generation of nuclear power plants), or the cylindrical graphite bricks that form the core of the Advanced Gas Reactors (widely employed in the United Kingdom), serving both as neutron moderator and structural components. In the latter case, years of neutron irradiation caused profound microscopic changes in the material that resulted in shrinking of the graphite bricks. But because the neutron bombardment does not spread evenly through the brick material, the rates of recession are also irregular. This causes tension and eventually cracking, affecting the safe operation of the power plants. Thus, a good characterization of the

* Corresponding author.
E-mail address: javier@cab.cnea.gov.ar (J. Dawidowski).

http://dx.doi.org/10.1016/j.nima.2015.01.055
0168-9002/

porosity of materials is particularly significant in graphites employed in the nuclear industry. Nuclear grade graphites are those with a density greater than 1.7 g/cm^3 (the theoretical value being 2.2 g/cm^3), which defines an upper bound on its porosity, that is an important parameter in reactor calculations.

Most of the methods to characterize the porosity of materials are based on adsorption properties [4]. Widely employed techniques are the mercury porosimetry, vapor–liquid equilibrium method [5], and liquid–solid thermoporometry [6]. The most popular method, known as the Brunauer–Emmett–Teller (BET) method [7], is based on gas adsorption. As this method is based on the area that is occupied by gas molecules, it is inaccurate either when the surface is too rough, or when the pores are too small or completely closed. Avnir et al. [8,9] found that the surfaces of most materials are fractals at the molecular size range. A consequence of this is that the routine analyses that employ the BET technique overestimate the effective area, since they consider an extra adsorption caused by the surface roughness. As an example, in the study of Kaneko et al. [10] BET measurements of the specific area in microporous carbons showed an overestimation of 40% due to capillary condensation. Besides the mentioned problem, the extra pressure applied to the gas can lead to pore deformation. On the other hand, microscopy techniques, besides not being representative of the whole volume, cannot be applied to microporous materials (pore sizes less than 2 nm).

The usual tools to explore the structure of solids and liquids in the nanometric scale are small angle X-ray and neutron scattering techniques (SAXS and SANS, respectively). While SAXS requires high-flux radiation facilities and good properties of longitudinal coherence (as provided by synchrotron radiation sources) and is sensitive to inhomogeneities in the electronic density of the sample, the SANS technique explores inhomogeneities in scattering length density and requires neutron facilities (e.g. reactors) to produce a monochromatic beam of cold neutrons. Both techniques explore the scale range from 1 to 100 nm and are applicable to both amorphous and crystalline materials. Some typical applications of SAXS and SANS include the determination of the pore size distribution and the estimation of the specific area in nanoparticulated systems.

As commented above, subthermal neutron transmission proved recently to be a tool to explore SANS effects. The interest in developing techniques based on neutron transmission is twofold. On the one hand it reinforces the role of small neutron facilities where this technique can be adequately implemented [11,2], while at high-flux sources high speed experiments can be performed, thus allowing real time studies during transformations. On the other hand, it can be adequately employed in neutron imaging data analysis. Energy- resolved neutron imaging has gained considerable interest over the last decade as a non-destructive tool to visualize distributions of different physical properties in macroscopic objects [12–18]. From the instrumental side this has been made possible due to advances in detector technology [19,20], the advent of more intense pulsed neutron sources and the development of dedicated monochromating devices at neutron imaging instruments of stationary neutron sources [21,22]. These advances in instrumentation have been accompanied by the development of basic physical models to interpret and analyze the energy-resolved neutron transmission of different material systems, in order to extract the information of interest from the transmitted neutron spectra. For polycrystalline materials it is possible to quantify crystallographic phases [23] and elastic deformation [24–26] and applied stresses [27], and to less extent texture and plastic deformation [16,28]. For single crystal materials, it is possible to determine the crystal orientation, mosaicity and elastic strain [29]. Neutron imaging techniques combined with grating interferometers have also been used to visualize the spatial distribution and quantify the signal due to ultrasmall-angle scattering within the sample [30].

In this paper we present a theoretical model to analyze the energy resolved neutron transmission signal that appears as a result of small-angle scattering within a sample. The proposed model allows the quantification of the spatial distributions in the nanometric range that exist within a sample. The model comprises a description of the pore sizes via a Log-Normal distribution and a form factor of spherical pores, and a standard description of the bulk solid. The contributions to the cross-section caused by the crystalline lattice (elastic coherent term) as well as the vibrational modes of the lattice (inelastic term) are considered through the NJOY code, and the contribution by 1-phonon coherent scattering is estimated according to the results of Al-Qasir [31]. We apply this model to characterize the pore distribution in nuclear graphite produced by different manufacturing techniques from energy resolved neutron transmission experiments. The experimental neutron work has been presented in a previous report [2], so it will be only briefly described in this paper. In order to assess the results of the procedure presented in this paper, we performed SAXS measurements at the LNLS (Campinas, Brazil) on the same systems. We compare the results from both methods.

2. Experimental

2.1. Samples

Three different types of graphite were examined in this work, needle-coke, pitch coke and isostatic-pressed graphite, which differ in the way they were manufactured:

- Needle coke graphite is the most porous species [32]. Samples were cut from a 24 cm cube provided by the RA-6 Nuclear Reactor, of the Centro Atómico Bariloche, Argentina. The density of the material is 1.681 ± 0.008 g/cm^3. Elemental composition determined by EXAFS is C 99.815%, S 0.102%, Ca 0.047%, Si 0.026%, Al 0.009%, and K 0.001%. Pores of around 1 mm are visible to the naked eye.
- Pitch-coke graphite is a byproduct of pitch produced by heat treatment, leading to more isometric particles than needle-coke graphite. The resulting material is more dense 1.725 ± 0.004 g/cm^3 than the needle coke graphite. Although the sample has a smoother surface than pitch coke graphite, pores are still visible to the naked eye. Spherical samples were machined out from a rod.
- Isostatic-pressed graphite is manufactured from finer coke particles, and has very uniform and isotropic properties, that makes it suitable to be used as neutron moderator. Spherical samples were molded by isostatic pressing. These samples presented the largest density (1.740 ± 0.004 g/cm^{-3}).

2.2. Experimental techniques

SAXS experiments, performed in transmission mode, were done in the SAXS1 beamline at the Laboratorio Nacional de Luz Sincrotron (LNLS) in Campinas, Brazil. The beamline works with a fixed energy of 8 keV and a beam size of 1.5 mm (horizontal) $\times$ 0.5 mm (vertical). The X-ray detection was performed with a solid state detector PILATUS 300 K with a resolution of $0.1(\delta E/E)$. To increase the statistics, the detection threshold was set at 7 keV. Two ranges of q were measured, $0.11\ \mathrm{nm}^{-1} < q < 4\ \mathrm{nm}^{-1}$ and $0.03\ \mathrm{nm}^{-1} < q < 1.5\ \mathrm{nm}^{-1}$, to cover the highest possible range of momentum transferred. Seven graphite samples were employed, four corresponding to needle-coke and three to pitch-coke.

The samples were sectioned to 0.7 mm width, with a PetroThin ® sectioning system. These thickness was chosen so an attenuation factor of 1/e for X-rays of 8 keV was obtained. The samples produced by this method had a rectangular shape of approximately 2 cm × 3 cm. In order to explore possible inhomogeneities of the porosity, squares of 3 mm × 3 mm were cut from the center and the edge of the samples.

The neutron transmission experiments were performed at the Bariloche electron linear accelerator (LINAC) facility (Argentina), and described in Refs. [2,33], so only a brief overview will be given here. A general scheme of the transmission experimental setup is shown in Fig. 1. The accelerator operated at a frequency of 50 Hz, and a 25-μA mean electron current. Neutrons were moderated in a 20 mm thick polyethylene slab. Measurements were carried out at room temperature, employing the "sample in-sample out" technique every 10 min. The detector bank consisted of seven ^{3}He proportional counters (10 atm filling pressure, 6 in. active length, 1 in. diameter) placed on the incident beam path at 8.27 m from the neutron source. The energy of the detected neutrons is determined by the time of flight method. The lower frame of Fig. 1 shows the incident spectrum as a function of the energy. The recorded spectra are rebinned in energy channels to optimize the statistics. Thus, the energy resolution in the thermal range, where the count rate is higher, is $\Delta E/E = 0.01$ whilst $\Delta E/E = 0.03$ in the subthermal range and $\Delta E/E = 0.05$ in the epithermal range. The sample was at a distance of 4.9 m from the detection bank. The neutron beam was collimated, so its cross-sectional diameter was 12.5 cm at the detection position.

3. Fundamentals of the method

According to Petriw et al. [2] the small angle contribution σ_{SANS} to the neutron total cross-section can be written as

$$\sigma_{SANS}(k_0) = \frac{1}{2k_0^2}\int_0^{2k_0} qI(q)\,dq, \tag{1}$$

where k_0 is the modulus of the incident wave vector, and $I(q)$ is the intensity of scattered neutrons at a momentum transfer q per atom, that depends only on the modulus of q for isotropic samples.

To calculate the small angle scattering contribution it is necessary to find an expression for $I(q)$ in terms of the porous structure. For the graphite samples studied in this work a model of spherical pores with a pore size distribution is employed. In this model, the *intensity of neutrons scattered by the sample (due to SANS effects)* $I'(q)$ can be calculated with the expression [34]

$$I'(q) = \int_0^\infty \left[(\Delta\rho)^2 v(r)^2 \frac{9(\sin(qr) - qr\cos(qr))^2}{(qr)^6}\right] N_p n(r)\,dr, \tag{2}$$

where $\Delta\rho$ is the commonly called contrast, i.e. the difference between the scattering length densities (for the system graphite–air $\Delta\rho$ is 7497×10^{-6} Å^{-2}), $v(r)$ is the volume of a pore with radius r, N_p is the total number of pores, $n(r)$ is the fraction of pores per radius interval between r and $r+dr$ (pore size distribution). The term between square brackets in Eq. (2) corresponds to the intensity scattered by a spherical pore of radius r.

To determine the *intensity of neutrons scattered per atom* $I(q)$, we must divide $I'(q)$ by the total number of carbon atoms N_C in the sample. The number of pores divided by the total number of atoms can be written as

$$\frac{N_p}{N_C} = \frac{N_p}{V_T}\frac{V_T}{N_C}, \tag{3}$$

where V_T is the total sample volume. If V_P is the total volume of pores in the sample and $\overline{v}_p$ the average pore volume, we can write

$$\frac{N_p}{V_T} = \frac{1}{\overline{v}_p}\frac{V_p}{V_T} = \frac{\phi}{\overline{v}_p}, \tag{4}$$

and

$$\overline{v}_p = \int_0^\infty \frac{4}{3}\pi r^3 n(r)\,dr, \tag{5}$$

where ϕ is the porosity defined as the ratio V_P/V_T. Furthermore, we can write

$$\frac{V_T}{N_C} = \frac{1}{n_C(1-\phi)}, \tag{6}$$

where n_C is the number of carbon atoms per unit of volume in an ideal material without pores. The total volume of the pores can be

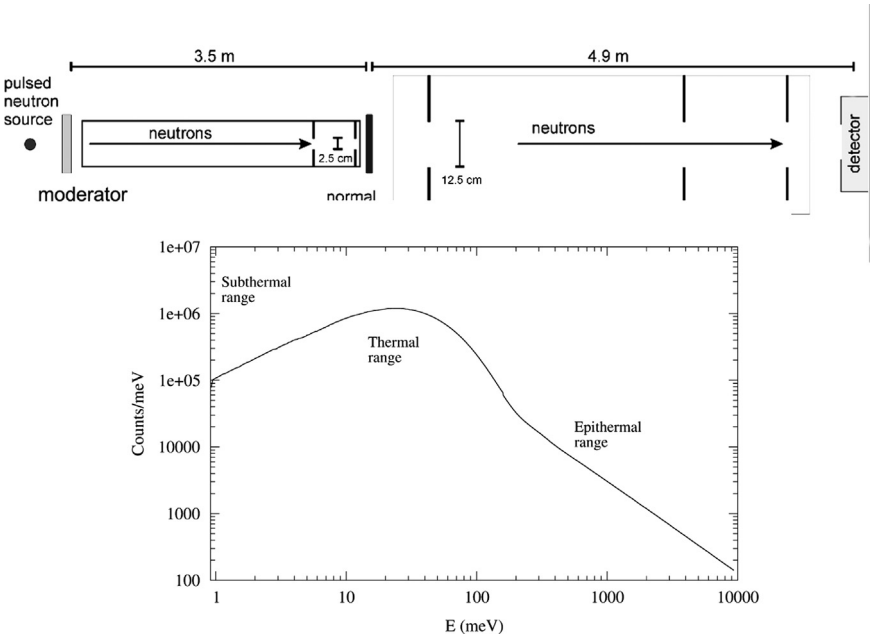

Fig. 1. (Top) General layout for the neutron transmission experiments performed in this work. (Bottom) Incident spectrum as a function of the energy. The intensity is expressed as the rate of number of counts over monitor counts.

evaluated through the theoretical ρ_t and measured ρ_m densities as

$$V_P = M\left(\frac{1}{\rho_m} - \frac{1}{\rho_t}\right). \quad (7)$$

with M being the sample mass. Now, using Eqs. (2)–(7) in the total cross-section of SANS (1), the following expression can be written as

$$\sigma_{SANS}(k_o) = \frac{1}{2k_o^2}\left[\frac{\phi}{\overline{v}_p n_c(1-\phi)}\right]\int_0^{2k_o}\int_0^{\infty}(\Delta\rho)^2 v(r)^2 \times \frac{9(\sin(qr) - qr\cos(qr))^2}{(qr)^6} n(r)_q \, dr \, dq. \quad (8)$$

In this work a log-normal pore radius distribution $n(r)$ was used:

$$n(r) = \exp\left(-\frac{1}{2}\frac{\left(\ln\frac{r}{r_0}\right)^2}{\sigma^2}\right)\frac{1}{r\sigma\sqrt{2\pi}}, \quad (9)$$

so the free parameters in Eq. (8) are the width of the pore size distribution (σ), and the maximum of the distribution (r_0).

4. Results and discussion

4.1. SAXS results

In Fig. 2(a), the normalized X-ray scattered intensities $I(q)$ for the different sections of pitch and needle coke samples in the measured range $0.03\ \text{nm}^{-1} < q < 0.1\ \text{nm}^{-1}$ are shown. A monotonous decrease of $I(q)$ as a function of the transferred momentum q is observed in all the samples, which indicates that no signature of a preferential pore size is observed. The curves that belong to the edge and center of the pitch coke sample show no evident differences. This fact indicates that the porosity is homogeneous in this material. In contrast, for the needle coke sample the intensities corresponding to the edge and center of the sample are clearly different, thus indicating a variation of the pore size, which could probably be caused by the manufacture method [35]. Plotting $\log(I(q))$ as a function of q^2, a nonlinear behavior is observed (both in pitch coke and needle coke samples), which is indicative that Guinier's law is not followed. The steep increase of the scattered intensity at very low angles is caused by inhomogeneities in the material on a larger scale [34].

An interpretation of the integral intensities of the $I(q)$ curves shown in Fig. 2 can be found in the theory of small angle scattering. We evaluated the integral value of $I(q)$ weighted by q^2, known as the Porod invariant [34], which can be related to the volume fraction of the pores ϕ as

$$Q = \int_0^{\infty} q^2 I(q)\, dq = 2\pi^2 \rho_c^2 \phi(1-\phi) \quad (10)$$

where ρ_c is the carbon electron density. Q-values evaluated by integration between the experimentally accessible upper and lower limits of q show that the ratio of the pore volume to the total volume is around 20%, consistently with the value determined by Eq. (7).

A closer examination of the curves shows interesting features to analyze. The asymptotic behavior of $I(q)$ for large q values can be represented as $I(q) \propto q^{-\alpha}$, where α is related to the roughness of the interface for a system composed of two electronic densities (for smooth surfaces a value of 4 is expected). The fitted α values were 3.496 ± 0.003 for needle coke and 3.411 ± 0.002 for pitch coke (see Fig. 2(b)). The fact that the values obtained are not integers and lower than 4 indicates a fractal surface behavior. The fractal surface dimensions, defined as $D_m = 6 - \alpha$ [37], are approximately equal to 2.5, which implies that the material has a rough pore–solid interface [38].

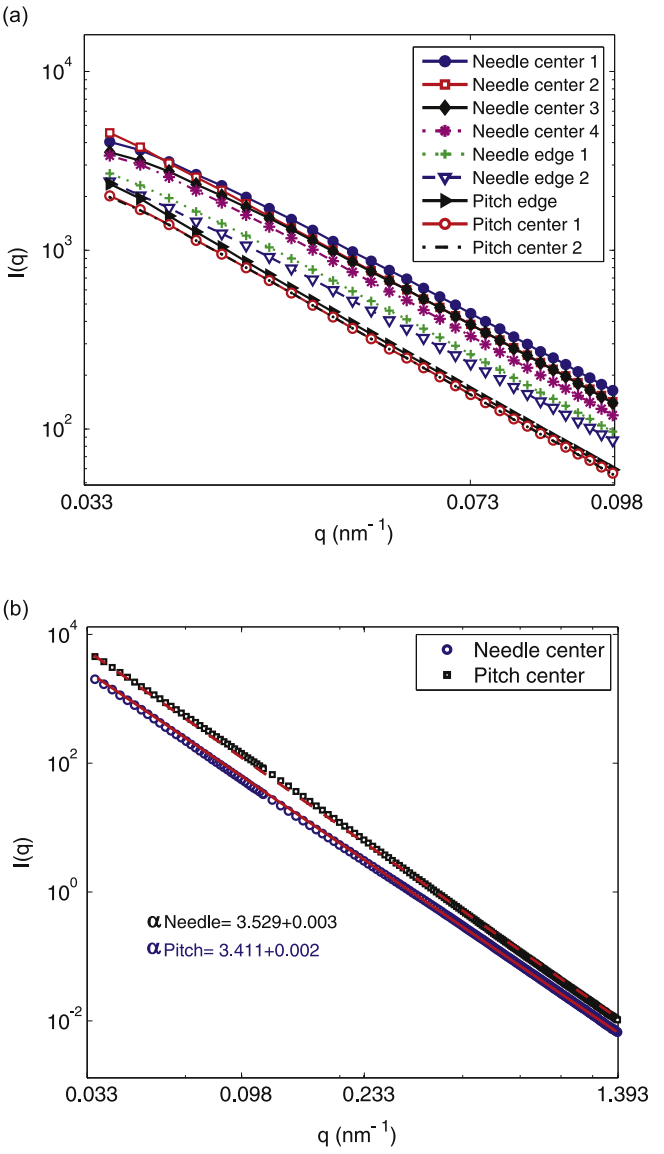

Fig. 2. (a) Experimental SAXS intensities for the different graphite samples, measured at different positions to check homogeneity of the samples. (b) A detail of two $I(q)$ curves to determine the fractal dimension. Note that in both graphs, both ordinates and abscissas are in logarithmic scale.

In order to determine a rough estimation of the pore size (which is useful as an initial parameter guess in subsequent refinements), the tangent method [36] was applied. This method consists in fitting a linear function in a suitable range where $I(q)$ behaves linearly with q^2. The slope of this line allows us to have an estimation of the representative pore radius. This method gave a radius of gyration of about 10 nm for all samples.

SAXS data were fitted with the SAXSFit software [39]. A model of spherical pores with a log-normal pore radius distribution was used (Eq. (9)). The center and the width of the distributions resulted in 41 ± 2 Å and 0.12 ± 0.05 Å, respectively, for pitch coke samples. For the needle coke samples the centers of the distributions were 27 ± 2 Å and 31 ± 2 Å at the center and the edge, respectively, whereas the widths were 0.11 ± 0.05 Å and 0.12 ± 0.05 Å.

4.2. Neutron transmission results

The total cross-section was calculated considering the various contributions existent in the wavelength range from 7 to 9 Å. On the one hand, the contributions from the crystal structure (elastic

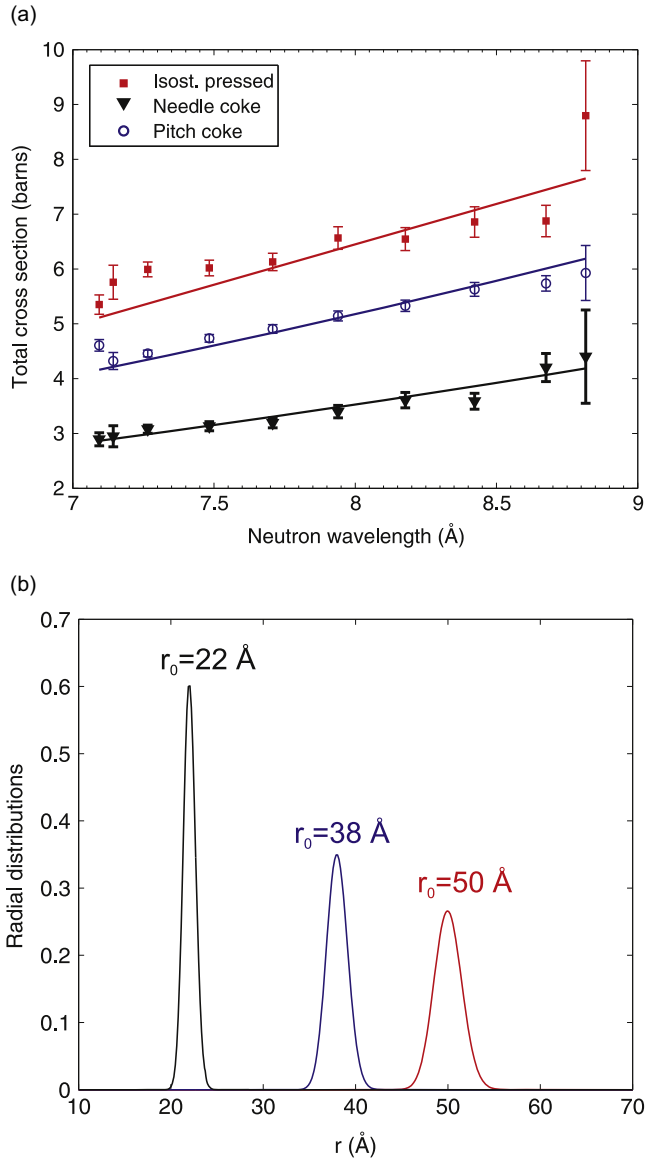

Fig. 3. (a) Experimental neutron total cross-section data (dots) as a function of neutron wavelength, and the corresponding fitted curves. (b) Pore distributions determined from Eq. (8), with the parameters shown in Table 1.

Table 1
SAXS and neutron transmission (NT) results.

Sample	SAXS		NT	
	r_0 (Å)	σ	r_0 (Å)	σ
Needle coke center	27 ± 2	0.11 ± 0.05	22 ± 1	0.03
Needle coke edge	31 ± 2	0.11 ± 0.05	–	–
Pitch coke	41 ± 2	0.12 ± 0.05	38 ± 1	0.03
Isostat. pressed	–	–	50 ± 1	0.03

coherent and incoherent terms), and vibrations (inelastic incoherent component) were calculated employing the NJOY code [3], resulting in about 0.5 barns per atom throughout the range of interest. On the other hand, the one-phonon coherent scattering was assessed, based on the work of Al-Qasir et al. [31], resulting in a contribution of about 0.3 barns per atom in the range of interest. Finally, the small angle scattering contribution was calculated from Eq. (8) keeping r_0 and σ as fitting parameters. The results of such fittings are shown in Fig. 3(a) and in Table 1. Due to the difficulty in the convergence process of σ, this value was kept fixed in a value where the parameter r_0 showed good convergence. The final values of r_0 were insensitive to changes in σ of about 30%. For this reason we report a representative value of σ without errors. In Fig. 3(b) we show the radial distributions (Eq. (9)), with the parameters fitted from neutron transmission data.

Comparative results between SAXS and Neutron Transmission are shown in Table 1. As can be seen, there is an agreement between the mean pore radii obtained with both techniques, and the pore distributions' widths (σ) employed to analyze Neutron Transmission data are lower, although relatively insensitive, what sets a limit in the ability of the Neutron Transmission technique to determine σ. This is a result of the dependency of the total cross-section on σ as evidenced by observing Eq. (8), where σ affects only the function $n(r)$. The integral in (8) is not very sensitive to a variation of σ. Thus, the parameter σ can be used only as a rough comparison of the polydispersion level between the samples studied.

5. Conclusions

In this paper we have shown that the subthermal neutron transmission technique has the capability to investigate small angle scattering effects. Its sensitivity to the pore size confers the Neutron Transmission the potential to be a useful tool for the study of materials at nanoscale. This is evidenced in the good compatibility of the values of the mean pore radii determined in this work with this technique and SAXS, which is established as a standard technique in the domain of nanoscales.

We must highlight that Eq. (8) formulated in this work constitutes a useful link between the intensity $I(q)$ observed in SANS experiments and the total cross-section (measured in barns), observed in neutron transmission experiments. In the analysis we showed that the form factors commonly used as trial functions in the SANS technique can also be adopted in neutron transmission data analysis. We envisage a wide field of applicability of this technique even in the case of the study of complex systems in which the density and the chemical composition are not clearly defined. In such case it is still possible to fit the form factor parameters and an overall scaling constant which is the factor in square brackets in Eq. (8).

The results shown in this work are in agreement with those reported in the literature for similar samples [36] employing SANS, which supports the soundness of the present results. Experiments of this kind can be performed quickly, permitting the scanning of large samples and allowing to perform experiments in small facilities. As a future prospect, we propose to employ the present data analysis procedure to determine the spatial variation of the porosity in large Graphite blocks using energy-resolved neutron imaging. This kind of studies could be performed with instruments like ENGIN-X (ISIS facility, United Kingdom) using an MCP detector [18], a field under promising development.

Acknowledgments

We gratefully acknowledge L. Capararo and F. Moreira for the technical support, and M. Schneebeli, P. DAvanzo and A. Mancilla for the LINAC operation at Bariloche and Laboratorio Nacional de Luz Sncrotron (LNLS), Brazil, for institutional support. This work was partially supported by ANPCyT (PICT 2011 - 534) and CONICET (PIP 11220110100552) (Argentina).

References

[1] J.R. Santisteban, A. Steuwer, L. Edwards, P.J. Withers, M.E. Fitzpatrick, Journal of Applied Crystallography 35 (4) (2002) 497. http://dx.doi.org/10.1107/S0021889802009044.

[2] S. Petriw, J. Dawidowski, J. Santisteban, Journal of Nuclear Materials 396 (2–3) (2010) 181. http://dx.doi.org/10.1016/j.jnucmat.2009.11.003.

[3] R.E. MacFarlane, D.W. Muir, The NJOY Nuclear Data Processing System, Version 91, Technical Report, Los Alamos National Laboratory, October 1994.

[4] T.J. Barton, L.M. Bull, W.G. Klemperer, D.A. Loy, B. McEnaney, M. Misono, P.A. Monson, G. Pez, G.W. Scherer, J.C. Vartuli, O.M. Yaghi, Chemistry of Materials 11 (10) (1999) 2633. http://dx.doi.org/10.1021/cm9805929.

[5] E.P. Barrett, L.G. Joyner, P.P. Halenda, Journal of the American Chemical Society 73 (1) (1951) 373. http://dx.doi.org/10.1021/ja01145a126.

[6] M. Brun, A. Lallemand, J.-F. Quinson, C. Eyraud, Thermochimica Acta 21 (1) (1977) 59.

[7] S. Brunauer, P.H. Emmett, E. Teller, Journal of the American Chemical Society 60 (2) (1938) 309. http://dx.doi.org/10.1021/ja01269a023.

[8] D. Avnir, D. Farin, P. Pfeifer, The Journal of Chemical Physics 79 (7) (1983) 3566.

[9] P. Pfeifer, D. Avnir, D. Farin, Surface Science 126 (1) (1983) 569.

[10] K. Kaneko, C. Ishii, Colloids and Surfaces 67 (1992) 203.

[11] J. Granada, J. Santisteban, J. Dawidowski, R. Mayer, Physics Procedia 26 (2012) 108, Proceedings of the First Two Meetings of the Union of Compact Accelerator-Driven Neutron Sources.

[12] E.H. Lehmann, G. Frei, P. Vontobel, L. Josic, N. Kardjilov, A. Hilger, W. Kockelmann, A. Steuwer, Nuclear Instruments and Methods in Physics Research Section A: Accelerators, Spectrometers, Detectors and Associated Equipment 603 (3) (2009) 429.

[13] L. Josic, E. Lehmann, A. Kaestner, Nuclear Instruments and Methods in Physics Research Section A: Accelerators, Spectrometers, Detectors and Associated Equipment 651 (1) (2011) 166. http://dx.doi.org/10.1016/j.nima.2010.12.120, Proceedings of the Ninth World Conference on Neutron radiography (The Big-5 on Neutron Radiography).

[14] R. Woracek, D. Penumadu, N. Kardjilov, A. Hilger, M. Strobl, R. Wimpory, I. Manke, J. Banhart, Journal of Applied Physics 109 (9) (2011) 093506.

[15] L. Josic, E. Lehmann, D. Mannes, N. Kardjilov, A. Hilger, Nuclear Instruments and Methods in Physics Research Section A: Accelerators, Spectrometers, Detectors and Associated Equipment 670 (2012) 68. http://dx.doi.org/10.1016/j.nima.2011.12.055.

[16] J. Santisteban, M. Vicente-Alvarez, P. Vizcaino, A. Banchik, S. Vogel, A. Tremsin, J. Vallerga, J. McPhate, E. Lehmann, W. Kockelmann, Journal of Nuclear Materials 425 (1–3) (2012) 218. http://dx.doi.org/10.1016/j.jnucmat.2011.06.043 (Microstructure Properties of Irradiated Materials).

[17] M. Strobl, R. Woracek, N. Kardjilov, A. Hilger, R. Wimpory, A. Tremsin, T. Wilpert, C. Schulz, I. Manke, D. Penumadu, Nuclear Instruments and Methods in Physics Research Section A: Accelerators, Spectrometers, Detectors and Associated Equipment 680 (2012) 27. http://dx.doi.org/10.1016/j.nima.2012.04.026.

[18] A.S. Tremsin, J.B. McPhate, A. Steuwer, W. Kockelmann, A. M Paradowska, J.F. Kelleher, J.V. Vallerga, O.H.W. Siegmund, W.B. Feller, Strain 48 (4) (2012) 296. http://dx.doi.org/10.1111/j.1475-1305.2011.00823.x.

[19] A.S. Tremsin, J.B. McPhate, J.V. Vallerga, O.H. Siegmund, W.B. Feller, E. Lehmann, A. Kaestner, P. Boillat, T. Panzner, U. Filges, Nuclear Instruments and Methods in Physics Research Section A: Accelerators, Spectrometers, Detectors and Associated Equipment 688 (2012) 32. http://dx.doi.org/10.1016/j.nima.2012.06.005.

[20] A.S. Tremsin, J.B. McPhate, A. Steuwer, W. Kockelmann, A.M. Paradowska, J.F. Kelleher, J.V. Vallerga, O.H.W. Siegmund, W.B. Feller, Strain 48 (4) (2012) 296. http://dx.doi.org/10.1111/j.1475-1305.2011.00823.x.

[21] M. Strobl, A. Hilger, M. Boin, N. Kardjilov, R. Wimpory, D. Clemens, M. Mühlbauer, B. Schillinger, T. Wilpert, C. Schulz, K. Rolfs, C. Davies, N. O'Dowd, P. Tiernan, I. Manke, Nuclear Instruments and Methods in Physics Research Section A: Accelerators, Spectrometers, Detectors and Associated Equipment 651 (1) (2011) 149. http://dx.doi.org/10.1016/j.nima.2010.12.121, Proceedings of the Ninth World Conference on Neutron Radiography (The Big-5 on Neutron Radiography).

[22] M. Schulz, P. Böni, E. Calzada, M. Mühlbauer, B. Schillinger, Nuclear Instruments and Methods in Physics Research Section A: Accelerators, Spectrometers, Detectors and Associated Equipment 605 (1–2) (2009) 33. http://dx.doi.org/10.1016/j.nima.2009.01.123, ITMNR 08 Proceedings of the Sixth Topical Meeting on Neutron Radiography.

[23] A. Steuwer, J. Santisteban, P. Withers, L. Edwards, Physica B: Condensed Matter 350 (1–3) (2004) 159. http://dx.doi.org/10.1016/j.physb.2004.04.018, Proceedings of the Third European Conference on Neutron Scattering.

[24] J.R. Santisteban, L. Edwards, A. Steuwer, P.J. Withers, Journal of Applied Crystallography 34 (3) (2001) 289. http://dx.doi.org/10.1107/S0021889801003260.

[25] J. Santisteban, L. Edwards, M. Fitzpatrick, A. Steuwer, P. Withers, M. Daymond, M. Johnson, N. Rhodes, E. Schooneveld, Nuclear Instruments and Methods in Physics Research Section A: Accelerators, Spectrometers, Detectors and Associated Equipment 481 (1–3) (2002) 765. http://dx.doi.org/10.1016/S0168-9002(01)01256-6.

[26] J.R. Santisteban, A. Steuwer, L. Edwards, P.J. Withers, M.E. Fitzpatrick, Journal of Applied Crystallography 35 (4) (2002) 497. http://dx.doi.org/10.1107/S0021889802009044.

[27] A. Steuwer, J.R. Santisteban, P.J. Withers, L. Edwards, M.E. Fitzpatrick, Journal of Applied Crystallography 36 (5) (2003) 1159. http://dx.doi.org/10.1107/S0021889803013748.

[28] J.R. Santisteban, L. Edwards, V. Stelmukh, Physica B: Condensed Matter 385–386 Part 1 (2006) 636. http://dx.doi.org/10.1016/j.physb.2006.06.090, Proceedings of the Eighth International Conference on Neutron Scattering.

[29] J.R. Santisteban, Journal of Applied Crystallography 38 (6) (2005) 934. http://dx.doi.org/10.1107/S0021889805028190.

[30] M. Strobl, C. Grünzweig, A. Hilger, I. Manke, N. Kardjilov, C. David, F. Pfeiffer, Physical Review Letters 101 (2008) 123902. http://dx.doi.org/10.1103/PhysRevLett.101.123902.

[31] I.I. Al-Qasir, A.I. Hawari, Transactions of the American Nuclear Society 96 (2007) 660.

[32] B.T. Kelly, B.J. Marsden, K. Hall, Irradiation Damage in Graphite due to Fast Neutrons in Fission and Fusion Systems, Technical Report, International Atomic Energy Agency, Vienna, Austria, 2000.

[33] A. Tartaglione, V. Galván, J. Dawidowski, F. Cantargi, J.J. Blostein, Journal of Instrumentation 8 (11) (2013) P11009.

[34] R.-J. Roe, Methods of X-ray and Neutron Scattering in Polymer Science, Oxford University Press, New York, 2000.

[35] Groupe français d'étude des carbones, Les Carbones: par le Groupe français d'étude des carbones, A.-M. Barrachin, M.J. Barriol, M. Bastick, L. Bonnetais, et al. Masson et Cie (Laval, impr. Barnéoud), 1965.

[36] Z. Mileeva, D.K. Ross, D. Wilkinson, S. King, T. Ryan, H. Sharrock, Carbon 50 (14) (2012) 5062. http://dx.doi.org/10.1016/j.carbon.2012.06.046.

[37] X. Du, E. Wu, Journal of Physics and Chemistry of Solids 68 (9) (2007) 1692. http://dx.doi.org/10.1016/j.jpcs.2007.04.013.

[38] L. Pajak, B. Bierska-Piech, J. Mrowiec-Bialon, A. Jarzebski, R. Diduszko, Fibers and Textiles in Eastern Europe 13 (2005) 69.

[39] B. Ingham, H. Li, E.L. Allen, M.F. Toney, SAXSFit: A Program for Fitting Small-Angle X-ray and Neutron Scattering Data, ArXiv e-prints: arXiv:0901.4782.